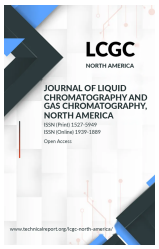

Journal of Liquid Chromatography and Gas Chromatography, North America
https://technicalreport.org/lcgcnam

LC GC N. Am., Vol. 43, No.3, 35-41, 2025

Technical Reports Press

RESEARCH ARTICLE

Endpoint-Resolved Ranking of Pd(II), ZrO(IV), and VO(IV) Schiff-Base Complexes: Separating Docking Affinity from Antimicrobial and HCT-116 Cytotoxic Potency

James Carter[1*]

[1]*Center for Chromatographic Research Midland Scientific University Canada*
[*]*Corresponding author*

Corresponding author:
james_carter29@gmail.com

Received: 23 November 2025
Accepted: 23 November 2025
Available online: 23 November 2025

Abstract

Metal coordination can substantially change the biological behavior of Schiff-base ligands, but antimicrobial inhibition, cancer-cell cytotoxicity, antioxidant response, DFT descriptors, and molecular docking are often interpreted as though they identify the same active compound. The reliability of that assumption was examined for a four-member tridentate imine series comprising H_2B and its ZrO(IV), VO(IV), and Pd(II) complexes. Numerical endpoints for inhibition zones and minimum inhibitory concentrations against *Escherichia coli*, *Micrococcus luteus*, *Aspergillus flavus*, and *Geotrichum candidum*; HCT-116 IC_{50} values; DPPH antioxidant ordering; DFT-derived reactivity descriptors; and docking energies for the 6KQ9 and 1R4U receptor models were harmonized into direction-corrected scores. Metalation improved the phenotypic profile relative to H_2B, with PdB giving the highest mean inhibition zone, highest mean activity index, lowest HCT-116 IC_{50} among the complexes, and strongest ordinal DPPH response. In contrast, VOB had the most favorable docking energies for both receptor models. The phenotype composite ranked PdB > ZrOB > VOB > H_2B, whereas the docking composite ranked VOB > ZrOB > PdB > H_2B. The resulting rank inversion demonstrates that docking affinity is not a direct surrogate for whole-cell antimicrobial or HCT-116 cytotoxic potency in this metal-complex panel. Sensitivity analysis further showed that PdB remains the preferred phenotypic candidate unless docking receives more than approximately one-third of the total prioritization weight, after which VOB becomes dominant. The work establishes a reproducible endpoint-resolved strategy for distinguishing phenotypic leads from receptor-binding candidates and defines the additional validation needed before mechanistic or therapeutic conclusions are drawn from compact bioinorganic screening datasets.

Keywords: Schiff base; bioinorganic chemistry; metal complexes; molecular docking; cytotoxicity; antimicrobial activity; endpoint harmonization; Pd(II); VO(IV); ZrO(IV)

1. Introduction

Schiff bases containing azomethine nitrogen and phenolic oxygen donor atoms are versatile ligands for transition-metal and oxometal coordination chemistry. Their biological relevance arises from the ability of metal coordination to alter electron density, donor-atom availability, molecular geometry, hydrolytic behavior, lipophilicity, redox reactivity, and interactions with cellular biomolecules [1–3]. These effects are strongly metal-dependent. The same parent ligand may display different antimicrobial, cytotoxic, antioxidant, and receptor-binding profiles after coordination to different metal centers, particularly when square-planar, square-pyramidal, and oxometal environments are compared within a single chemical series [4–6].

A tridentate imine ligand derived from 2-amino-3-hydroxypyridine and 5-bromosalicylaldehyde has been examined with ZrO(IV), VO(IV), and Pd(II) centers by spectroscopy, thermal analysis, powder X-ray

Cite as: J. Carter (2025). Endpoint-Resolved Ranking of Pd(II), ZrO(IV), and VO(IV) Schiff-Base Complexes: Separating Docking Affinity from Antimicrobial and HCT-116 Cytotoxic Potency. LC GC N. Am., 43(3) (2025) 35-41.

diffraction, magnetic susceptibility, DFT calculations, antimicrobial assays, DPPH radical-scavenging measurements, HCT-116 cytotoxicity testing, and docking against microbial receptor models [7]. The chemical assignments support a dibasic ONO donor mode for H_2B, square-pyramidal structures for ZrOB and VOB, and a square-planar structure for PdB. The biological results also show a general increase in activity after metal coordination. A more detailed comparison, however, reveals that the endpoint order is not uniform: PdB gives the strongest overall phenotypic response across several biological measures, whereas VOB gives the most favorable docking energies for both the *M. luteus* 6KQ9 and *A. flavus* 1R4U receptor models [7].

This divergence is mechanistically important. If docking energy were an adequate proxy for biological potency, the strongest predicted receptor binder would also be expected to dominate the antimicrobial and cytotoxic endpoints. Whole-cell potency instead depends on additional processes that are not represented in static docking calculations, including agar diffusion, membrane permeation, solubility, aggregation, complex stability, aquation, ligand exchange, intracellular accumulation, efflux, redox cycling, and interactions with multiple biomolecular targets. Docking remains useful for generating receptor-binding hypotheses, but docking scores are sensitive to receptor preparation, ligand protonation, conformational sampling, solvation treatment, scoring functions, and the absence of cellular barriers [8, 9]. A metal-complex series is therefore more informative when in vitro and in silico endpoints are compared explicitly rather than assumed to be concordant.

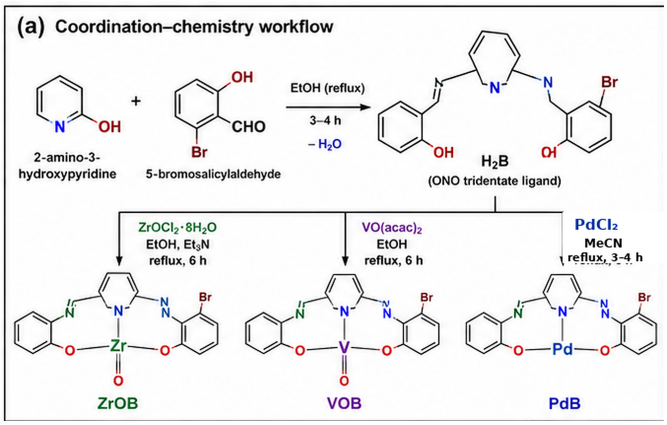

Figure 1: Chemical context of the H_2B–ZrOB–VOB–PdB panel. The scheme summarizes imine formation and subsequent metal coordination to the ZrO(IV), VO(IV), and Pd(II) complexes used for endpoint-resolved comparison.

The aim of this work is to define an endpoint-resolved ranking of the H_2B–ZrOB–VOB–PdB panel. The specific contributions are fourfold. First, all available biological and computational endpoints are transformed into direction-corrected scores so that antimicrobial zones, MICs, activity indices, HCT-116 IC_{50} values, DPPH ordering, DFT descriptors, and docking energies can be compared on a common scale. Second, ligand-normalized metalation gains quantify how much each metal center improves activity relative to H_2B. Third, rank-discordance analysis separates phenotypic potency from receptor-affinity hypotheses. Fourth, weight-sensitive prioritization shows how the selected lead changes when biological decision-making shifts from phenotype-dominant to docking-dominant criteria. This design provides a transparent route for extracting mechanistic value from compact bioinorganic datasets while preserving the limits of the available experimental evidence.

2. Materials and methods

2.1. Analytical dataset

The numerical matrix comprised four compounds: H_2B, ZrOB, VOB, and PdB [7]. The extracted endpoints included antimicrobial inhibition zones with standard deviations against *E. coli*, *M. luteus*, *A. flavus*, and *G. candidum*; MICs for the same organisms; activity-index percentages relative to ofloxacin for bacteria and fluconazole for fungi; HCT-116 MTT IC_{50} values; DPPH antioxidant potency order; selected DFT descriptors; and docking energies for the *M. luteus* receptor model 6KQ9 and the *A. flavus* receptor model 1R4U. The antimicrobial assays used 20 μg mL^{-1} solutions in DMSO, 24 h bacterial incubation at 37 °C, and 72 h fungal incubation at 35 °C. The cytotoxicity experiment used HCT-116 colon carcinoma cells, 24 h compound exposure, MTT viability measurement, and graphical IC_{50} estimation. The DPPH experiment used concentrations from 0 to 1280 μg mL^{-1}. The docking protocol included receptor preparation and validation by redocking, with an RMSD below 2 Å [7].

DPPH IC_{50} values were represented graphically and by potency order rather than as exact numerical values. To avoid unsupported precision, antioxidant activity was encoded as an ordinal endpoint with PdB ranked highest, followed by VOB, ZrOB, and H_2B, matching the stated order of IC_{50} values [7]. No primary composite score used estimated values digitized from the graph.

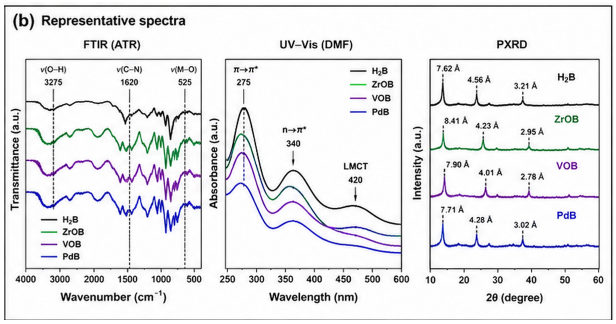

Figure 2: Representative visualization of characterization endpoints for the H_2B ligand and its metal complexes. The panel summarizes FTIR, UV–Vis, and PXRD-style evidence used to support coordination and structural differentiation; quantitative endpoint ranking in this manuscript is based on the numerical matrix in Table 1.

2.2. Experimental validation basis

The endpoint set contains three internal validation layers. First, antimicrobial activity is represented by both inhibition-zone measurements and MICs. Zone diameters are diffusion-dependent and can be influenced by compound mobility in agar, whereas MICs provide a concentration-based growth-inhibition measure; retaining both endpoints reduces the risk of selecting a lead from diffusion behavior alone [10]. Second, activity-index values anchor the microbial response to ofloxacin and fluconazole, allowing the metal complexes to be compared against assay-specific reference drugs. Third, HCT-116 cytotoxicity, DPPH scavenging, DFT descriptors, and docking scores provide orthogonal information on cellular viability, radical-scavenging behavior, electronic structure, and receptor-binding hypotheses [8, 9, 11–15]. These validation layers do not prove a single biological mechanism, but they support a controlled endpoint-resolved comparison within the same chemical panel.

2.3. Endpoint direction correction and normalization

Endpoints were transformed so that larger normalized values consistently represented stronger performance. Inhibition-zone diameter, activity-index percentage, docking-strength magnitude, electrophilicity index, and softness were treated as high-benefit variables. MIC and HCT-116 IC_{50} were treated as low-benefit variables. For high-benefit endpoint j, the normalized score for compound i was calculated as

$$Z_{ij} = \frac{x_{ij} - \min(x_j)}{\max(x_j) - \min(x_j)}. \quad (1)$$

For low-benefit endpoint j, the normalized score was calculated as

$$Z_{ij} = \frac{\max(x_j) - x_{ij}}{\max(x_j) - \min(x_j)}. \quad (2)$$

For the four-level ordinal DPPH endpoint, the normalized score was

$$Z_{ij} = \frac{4 - r_{ij}}{3}, \quad (3)$$

where $r = 1$ denotes the strongest DPPH scavenger. This procedure yields values between 0 and 1 within the four-compound panel. A value of 0 therefore denotes the lowest value within the panel, not absence of biological activity.

2.4. Metalation gain

Ligand-normalized gain quantified the magnitude by which each complex changed a given endpoint relative to H_2B. For high-benefit quantitative endpoints, percentage gain was calculated as

$$G_{ij} = 100 \times \frac{q_{ij} - q_{H_2B,j}}{q_{H_2B,j}}. \quad (4)$$

For MIC and IC_{50} endpoints, reciprocal potency values were used before gain calculation so that larger values corresponded to stronger activity:

$$q_{ij} = \frac{1}{\mathrm{MIC}_{ij}} \quad \text{or} \quad q_{ij} = \frac{1}{\mathrm{IC}_{50,ij}}. \quad (5)$$

DPPH was not expressed as a percentage gain because it was handled as an ordinal endpoint.

2.5. Composite scores and rank discordance

A phenotype composite (P_i) was defined as the arithmetic mean of normalized inhibition-zone, MIC, activity-index, HCT-116 cytotoxicity, and DPPH scores:

$$P_i = \frac{1}{5}\left(Z_{i,\mathrm{zone}} + Z_{i,\mathrm{MIC}} + Z_{i,\mathrm{AI}} + Z_{i,\mathrm{HCT116}} + Z_{i,\mathrm{DPPH}}\right). \quad (6)$$

A docking composite (D_i) was defined as the mean of normalized docking-strength magnitudes for 6KQ9 and 1R4U:

$$D_i = \frac{1}{2}\left(Z_{i,6\mathrm{KQ9}} + Z_{i,1\mathrm{R4U}}\right). \quad (7)$$

Rank discordance was calculated as

$$\Delta R_i = R(P_i) - R(D_i), \quad (8)$$

where rank 1 denotes the highest score. Negative values indicate phenotype-favored compounds, whereas positive values indicate docking-favored compounds.

2.6. Lead-prioritization sensitivity

A weighted prioritization score was used to determine whether lead selection depended on the relative importance assigned to phenotypic potency and docking affinity:

$$S_i(\alpha) = (1 - \alpha)P_i + \alpha D_i, \quad (9)$$

where α ranges from 0 for fully phenotype-driven selection to 1 for fully docking-driven selection. The crossover point between leading compounds was identified by evaluating $S_i(\alpha)$ across $0 \le \alpha \le 1$.

2.7. Statistical scope and reproducibility

The panel size is appropriate for mechanistic ranking and endpoint integration but not for regression modeling, external prediction, or parametric hypothesis testing. Accordingly, the analysis relies on direction-corrected scaling, ligand-normalized gain, rank comparison, and sensitivity analysis rather than overfitted statistical models. The absence of raw replicate-level values for all endpoints also limits formal uncertainty propagation across the complete composite. Inhibition-zone standard deviations were used qualitatively to verify that the reported experimental variation was small relative to the major ligand-to-complex shifts, while MIC, HCT-116, DPPH, DFT, and docking outcomes were handled as endpoint-level values. Quantitative ranking figures were generated from the numerical matrix described in Table 1. Graphical chemistry, spectral, cytotoxicity, and docking panels provide visual context for the same compound series and are not used as additional numerical inputs to the composite scores.

3. Results

3.1. Endpoint matrix and derived summary

The four-compound panel spans one free ligand and three metal-centered structures. Characterization data assign square-pyramidal geometries to ZrOB and VOB and a square-planar geometry to PdB. Magnetic measurements identify VOB as paramagnetic and ZrOB and PdB as diamagnetic [7]. These structural differences provide a chemically meaningful basis for comparing endpoint behavior.

Table 1 summarizes the analytical matrix used for endpoint integration. Across the four microorganisms, mean inhibition-zone diameter increased from 20.75 mm for H_2B to 24.25 mm for ZrOB, 23.50 mm for VOB, and 25.25 mm for PdB. Mean MIC decreased from 7.00 μg mL^{-1} for H_2B to 4.00 μg mL^{-1} for ZrOB and PdB and 4.50 μg mL^{-1} for VOB. Mean activity index followed the same phenotypic direction, with PdB giving the largest mean activity index. HCT-116 cytotoxicity also favored PdB, whose IC_{50} was 12.66 μg mL^{-1}, compared with 20.96 μg mL^{-1} for ZrOB, 24.79 μg mL^{-1} for VOB, and 62.06 μg mL^{-1} for H_2B. The values support a general metalation effect and show that the magnitude of improvement depends on both the metal center and the endpoint.

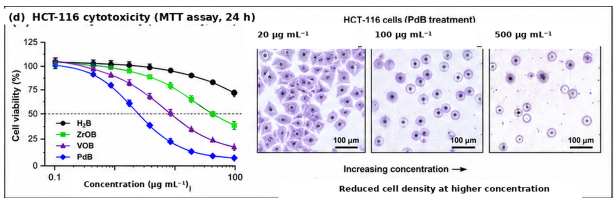

Figure 3: HCT-116 cytotoxicity visualization for the H_2B–ZrOB–VOB–PdB series. The dose–response plot reflects the endpoint ordering used in the IC_{50} analysis, and the microscopy-style panels summarize the concentration-dependent reduction in cell density observed under increasing treatment.

Table 1: Derived analytical matrix for endpoint-resolved comparison of H_2B and its metal complexes. Docking strength is the absolute magnitude of the reported negative docking energy; higher values indicate stronger predicted binding. DPPH is ordinal because exact antioxidant IC_{50} values were not tabulated.

Compound	Geometry	Mean zone (mm)	Mean MIC (μg mL^{-1})	Mean AI (%)	HCT-116 IC_{50} (μg mL^{-1})	DPPH rank	6KQ9 strength (kcal mol^{-1})	1R4U strength (kcal mol^{-1})
H_2B	free ligand	20.75	7.00	79.21	62.06	4	7.70	4.30
ZrOB	square pyramidal	24.25	4.00	92.25	20.96	3	36.50	34.80
VOB	square pyramidal	23.50	4.50	89.51	24.79	2	53.40	53.30
PdB	square planar	25.25	4.00	96.12	12.66	1	27.60	17.40

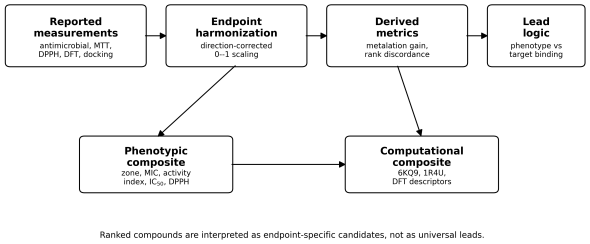

Figure 4: Endpoint-resolved workflow used to separate phenotypic potency from receptor-binding hypotheses. Measurements were harmonized by endpoint direction, converted into ligand-normalized and rank-based measures, and evaluated through phenotype and docking composites.

3.2. Metalation improves phenotypic potency but does not produce a uniform metal order

Ligand-normalized gains reveal the magnitude of coordination effects. Relative to H_2B, mean inhibition-zone diameter increased by 16.9% for ZrOB, 13.3% for VOB, and 21.7% for PdB. Reciprocal mean-MIC potency increased by 75.0% for ZrOB, 55.6% for VOB, and 75.0% for PdB. HCT-116 reciprocal cytotoxic potency increased by approximately 196% for ZrOB, 150% for VOB, and 390% for PdB. These gains demonstrate that metal coordination enhances biological performance relative to the free ligand, while the metal-dependent pattern differs among endpoints.

Organism-level inspection confirms endpoint specificity. PdB produced the largest inhibition zones for all four organisms, but MIC values identify different or shared leaders depending on the strain. PdB and VOB showed the lowest MIC against *E. coli*; ZrOB gave the lowest MIC against *M. luteus* and *A. flavus*; and PdB gave the lowest MIC against *G. candidum*. The MIC data therefore prevent zone diameter alone from defining the antimicrobial lead.

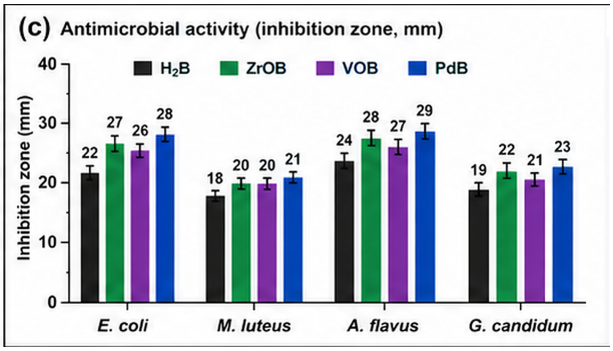

Figure 5: Whole-organism antimicrobial inhibition-zone response across the four tested strains. PdB gives the largest inhibition zones in the disk-diffusion readout, whereas MIC values identify organism-specific lead behavior.

3.3. Docking affinity separates VOB from the phenotypic lead

The most pronounced divergence occurs when docking scores are compared with whole-cell phenotypic endpoints. VOB had the strongest predicted binding to both microbial receptor models, with docking energies of -53.4 kcal mol^{-1} for 6KQ9 and -53.3 kcal mol^{-1} for 1R4U. ZrOB ranked second for both docking targets, whereas PdB ranked third. This order differs from the phenotypic ranking that favors PdB.

The normalized endpoint profile in Fig. 6 displays this separation. PdB reaches the maximum score for inhibition-zone response, MIC, activity index, HCT-116 cytotoxicity, and ordinal DPPH scavenging, but it is not the docking leader. VOB reaches the maximum score for both receptor-docking endpoints and electrophilicity but is lower than PdB on the integrated phenotypic endpoints. ZrOB occupies an intermediate position, combining strong MIC performance, high softness, and balanced docking behavior.

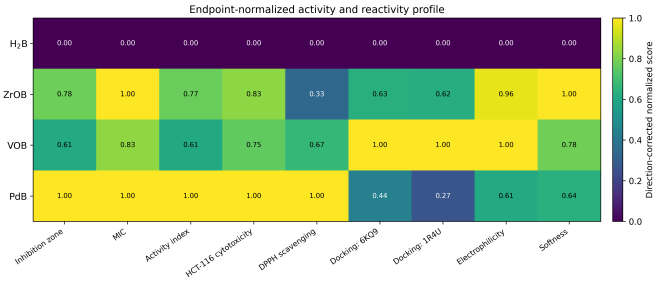

Figure 6: Direction-corrected normalized profile for the ligand and three complexes. Scores are scaled within the four-compound panel; 1 indicates the strongest value and 0 indicates the weakest value for that endpoint. DPPH is encoded as ordinal potency based on the IC_{50} order.

3.4. Phenotype and docking composites identify different lead complexes

Composite scores confirm that phenotypic potency and receptor-affinity ranking are not equivalent (Table 2). The phenotype composite ranked PdB first, ZrOB second, VOB third, and H_2B fourth. The docking composite ranked VOB first, ZrOB second, PdB third, and H_2B fourth. Rank-discordance analysis gave $\Delta R = -2$ for PdB and $\Delta R = +2$ for VOB. Thus, PdB is phenotype-favored relative to its docking rank, whereas VOB is docking-favored relative to its phenotype rank.

3.5. DFT descriptors provide mechanistic plausibility but not a single causal explanation

Selected DFT descriptors support the view that complexation changes the electronic profile of the ligand. H_2B had a HOMO–LUMO gap of 3.4228 eV, whereas the reported gaps for the complexes were lower: 3.1254 eV for ZrOB, 3.1854 eV for VOB, and 3.2271 eV for PdB.

Table 2: Composite scores and rank discordance. Negative rank-discordance values indicate phenotype-favored compounds; positive values indicate docking-favored compounds.

Compound	Phenotype score	Phenotype rank	Docking score	Docking rank	ΔR
H_2B	0.000	4	0.000	4	0
ZrOB	0.743	2	0.626	2	0
VOB	0.695	3	1.000	1	+2
PdB	1.000	1	0.351	3	−2

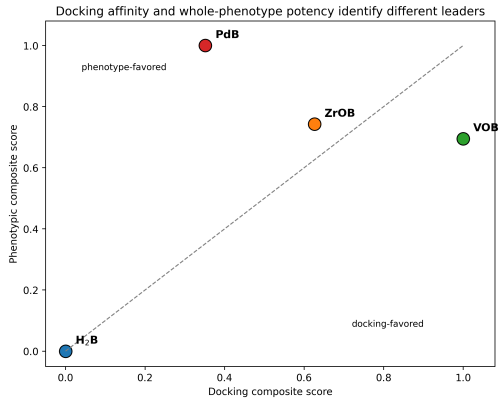

Figure 7: Phenotype composite score plotted against docking composite score. PdB is favored by phenotypic endpoints, whereas VOB is favored by docking affinity. The diagonal indicates equal normalized phenotype and docking scores.

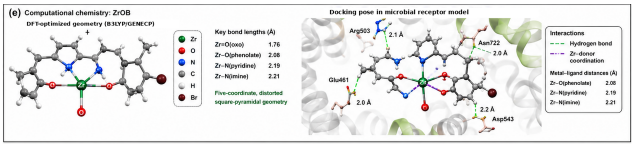

Figure 8: Representative computational visualization for the oxometal Schiff-base series. ZrOB is shown as a model five-coordinate oxometal complex together with a docking-pose representation of metal-complex contacts in a microbial receptor model. Quantitative docking interpretation is based on the 6KQ9 and 1R4U energies summarized in Table 1.

Electrophilicity increased from 3.5198 for H_2B to 5.8024 for ZrOB, 5.8924 for VOB, and 4.9715 for PdB. Softness also increased after metalation, with ZrOB highest in softness and VOB highest in electrophilicity. These changes are consistent with coordination-induced redistribution of electronic density and altered interaction potential.

The DFT descriptors do not uniquely predict the phenotypic leader. VOB has the highest electrophilicity and strongest docking profile, whereas PdB has the strongest phenotypic profile. This separation indicates that electronic reactivity and receptor-binding estimates are mechanistically relevant but insufficient to explain whole-cell potency without additional information on permeability, medium stability, aquation or ligand-exchange behavior, intracellular accumulation, and redox cycling.

3.6. Lead selection depends on the intended biological decision

Weighted prioritization shows how the preferred compound changes with the decision context (Fig. 9). When selection is fully phenotype-driven ($\alpha = 0$), PdB is the lead. When selection is fully docking-driven ($\alpha = 1$), VOB is the lead. The PdB–VOB crossover occurs at approximately $\alpha = 0.32$, meaning that VOB becomes preferred when receptor docking contributes more than about one-third of the total prioritization score. ZrOB remains a balanced but non-leading option under the equal-weight score, and H_2B remains lowest because all comparisons are scaled within the four-compound panel.

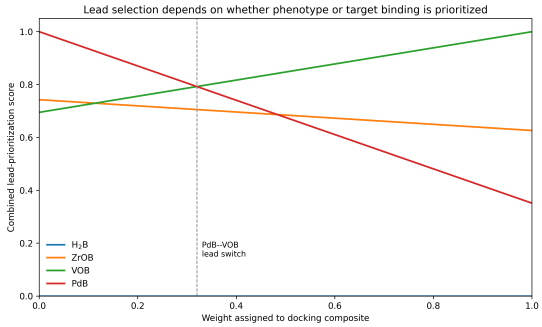

Figure 9: Lead-prioritization sensitivity as docking weight increases from 0 to 1. PdB is favored under phenotype-dominant weighting, whereas VOB becomes favored when docking receives more than approximately one-third of the total weight.

4. Discussion

4.1. Biological potency is endpoint-dependent

The integrated results show that coordination of the tridentate imine ligand to ZrO(IV), VO(IV), and Pd(II) improves biological performance relative to the free ligand, but the best complex depends on how potency is defined. PdB is the broad phenotypic leader across inhibition-zone response, activity-index response, HCT-116 cytotoxicity, and DPPH ordinal potency. VOB is the docking leader for both 6KQ9 and 1R4U. ZrOB is a balanced complex with strong MIC performance and favorable electronic softness but does not dominate either composite.

This endpoint dependence has practical significance. Metal-complex screening studies often present biological and computational assays in parallel, and the strongest value in one domain is sometimes used to support activity in another. The present results show that such inference can be misleading even within a small and chemically coherent series. Docking can identify plausible receptor-binding modes, but whole-cell antimicrobial and cytotoxic outcomes also reflect transport, stability, speciation, and multimodal cellular interactions.

4.2. PdB as the phenotypic lead

Pd(II) complexes can exhibit biological activity through mechanisms that do not require the strongest docking score against a single receptor. Square-planar Pd(II) compounds may interact with nitrogen- and sulfur-containing biomolecules, alter DNA or protein function, perturb membrane-associated processes, and influence oxidative stress depending on ligand environment and kinetic stability [2, 5]. In this panel, PdB may benefit from square-planar geometry, favorable ligand delocalization, and cell-entry properties that are not captured by static protein docking. Its lower docking rank is therefore compatible with strong phenotypic performance and suggests that whole-cell potency may arise from multiple contributing mechanisms.

The HCT-116 endpoint reinforces this interpretation. PdB reduced the IC_{50} from 62.06 μg mL^{-1} for H_2B to 12.66 μg mL^{-1}, a larger reciprocal potency gain than those observed for ZrOB and VOB. Because no normal-cell comparator is available, this cytotoxicity should not be interpreted as cancer selectivity. It does, however, identify PdB as the most active compound in the HCT-116 endpoint and as the most appropriate candidate for selectivity-index measurement in subsequent work.

4.3. VOB as the docking-led mechanistic candidate

The vanadyl complex shows the highest docking-strength magnitudes for both microbial receptor models and the highest electrophilicity

index in the DFT descriptor set. These properties indicate strong predicted capacity for polar, ionic, and donor–acceptor interactions at receptor active sites. For 1R4U, the docking table includes interactions involving GLU259 and LYS171 for VOB; for 6KQ9, it includes interactions involving ARG234 [7]. These contacts are consistent with the favorable predicted affinity.

The separation between docking and whole-cell potency can arise because docking evaluates a simplified target-binding event. Whole-cell antimicrobial response depends on solubility, aggregation, diffusion through agar, microbial envelope structure, intracellular accumulation, efflux, metal exchange, ligand release, and redox processes. A compound can bind strongly to an isolated receptor model yet reach the biological site of action inefficiently. VOB should therefore be considered a receptor-binding candidate that requires biochemical or biophysical target validation rather than the automatic antimicrobial lead.

4.4. ZrOB as a balanced intermediate

ZrOB ranks second in both phenotype and docking composites and displays the highest DFT softness in the selected descriptor set. It also gives the lowest MIC against *A. flavus* and *M. luteus*. This profile may be valuable where balanced activity and oxometal stability are preferred over maximal cytotoxicity. ZrOB should therefore remain in the development set, particularly for fungal MIC-focused follow-up and for experiments that introduce toxicity, selectivity, or stability constraints.

4.5. Implications for bioinorganic screening

The results support three principles for metallodrug and antimicrobial screening. First, endpoint integration should maintain the distinction between phenotypic activity and target-binding hypotheses. Second, metalation gain should be reported relative to the parent ligand so that the contribution of coordination is explicit. Third, lead selection should be treated as a decision problem rather than as a universal ranking. A compound selected for broad antimicrobial inhibition may differ from one selected for receptor binding, antioxidant response, or cancer-cell cytotoxicity.

For this panel, PdB is the most suitable phenotypic lead for follow-up antimicrobial and HCT-116 experiments. VOB is the most suitable docking-led candidate for receptor validation. ZrOB is the most balanced compound and deserves attention in fungal MIC-focused testing. These distinctions provide a more actionable interpretation than a single statement that metal complexes are more active than the ligand.

5. Conclusions

Endpoint-resolved analysis of the H_2B, ZrOB, VOB, and PdB Schiff-base panel shows that metal coordination enhances biological performance without producing a single universal activity ranking. PdB is the strongest phenotypic candidate across antimicrobial zones, activity indices, HCT-116 cytotoxicity, and ordinal DPPH response. VOB is the strongest docking candidate against both microbial receptor models. ZrOB provides a balanced profile with strong MIC and intermediate docking behavior. The rank inversion between PdB and VOB demonstrates that static docking affinity should not be used as a direct surrogate for whole-cell antimicrobial or HCT-116 cytotoxic potency in compact metal-complex series. Direction-corrected endpoint scoring, ligand-normalized metalation gain, rank-discordance analysis, and weight-sensitive prioritization provide a practical strategy for separating screening leads from receptor-binding candidates in Schiff-base bioinorganic chemistry.

References

[1] Abu-Dief, A. M., & Mohamed, I. M. A. (2015). A review on versatile applications of transition metal complexes incorporating Schiff bases. *Beni-Suef University Journal of Basic and Applied Sciences*, *4*, 119–133.

[2] Ndagi, U., Mhlongo, N., & Soliman, M. E. (2017). Metal complexes in cancer therapy: An update from drug design perspective. *Drug Design, Development and Therapy*, *11*, 599–616.

[3] Anthony, E. J., Bolitho, E. M., Bridgewater, H. E., Carter, O. W. L., Donnelly, J. M., Imberti, C., Lant, E. C., Lermyte, F., Needham, R. J., Palau, M., Sadler, P. J., Shi, H., Wang, F.-X., Zhang, W.-Y., & Zhang, Z. (2020). Metallodrugs are unique: Opportunities and challenges of discovery and development. *Chemical Science*, *11*, 12888–12917.

[4] Pessoa, J. C., Etcheverry, S., & Gambino, D. (2015). Vanadium compounds in medicine. *Coordination Chemistry Reviews*, *301–302*, 24–48.

[5] Medici, S., Peana, M., Nurchi, V. M., Lachowicz, J. I., Crisponi, G., & Zoroddu, M. A. (2015). Noble metals in medicine: Latest advances. *Coordination Chemistry Reviews*, *284*, 329–350.

[6] Oveisi Keikha, A., Shahraki, S., Dehghanian, E., & Mansouri-Torshizi, H. (2025). Effect of central metal ion on some pharmacological properties of new Schiff base complexes: Anticancer, antioxidant, kinetic/thermodynamic, and computational studies. *Spectrochimica Acta Part A: Molecular and Biomolecular Spectroscopy*, *325*, 125034.

[7] Abdel-Fatah, S. M., Basha, M. T., Al-Sulami, A. I., Shehata, M. R., & Abdel-Rahman, L. H. (2026). Synthesis, characterization, and antitumor potency of Pd^{2+}, ZrO^{2+}, and VO^{2+} complexes with tridentate Schiff base: In vitro biological and in-silico insights. *BMC Chemistry*, *20*, 112.

[8] Kitchen, D. B., Decornez, H., Furr, J. R., & Bajorath, J. (2004). Docking and scoring in virtual screening for drug discovery: Methods and applications. *Nature Reviews Drug Discovery*, *3*, 935–949.

[9] Warren, G. L., Andrews, C. W., Capelli, A.-M., Clarke, B., LaLonde, J., Lambert, M. H., Lindvall, M., Nevins, N., Semus, S. F., Senger, S., Tedesco, G., Wall, I. D., Woolven, J. M., Peishoff, C. E., & Head, M. S. (2006). A critical assessment of docking programs and scoring functions. *Journal of Medicinal Chemistry*, *49*, 5912–5931.

[10] Balouiri, M., Sadiki, M., & Ibnsouda, S. K. (2016). Methods for in vitro evaluating antimicrobial activity: A review. *Journal of Pharmaceutical Analysis*, *6*, 71–79.

[11] Mosmann, T. (1983). Rapid colorimetric assay for cellular growth and survival: Application to proliferation and cytotoxicity assays. *Journal of Immunological Methods*, *65*, 55–63.

[12] Blois, M. S. (1958). Antioxidant determinations by the use of a stable free radical. *Nature*, *181*, 1199–1200.

[13] Becke, A. D. (1993). Density-functional thermochemistry. III. The role of exact exchange. *Journal of Chemical Physics*, *98*, 5648–5652.

[14] Lee, C., Yang, W., & Parr, R. G. (1988). Development of the Colle–Salvetti correlation-energy formula into a functional of the electron density. *Physical Review B*, *37*, 785–789.

[15] Hay, P. J., & Wadt, W. R. (1985). Ab initio effective core potentials for molecular calculations. Potentials for the transition metal atoms Sc to Hg. *Journal of Chemical Physics*, *82*, 270–283.